Progress In Electromagnetics Research C, Vol. 133, 219–231, 2023

Enhancement of the Peak Power Handling Capability in Microstrip Filters by Employing Smooth-Profiled Conductor Strips

Jamil Ahmad[1, *], Jabir Hussain[1], Ivan Arregui[1], Petronilo Martin-Iglesias[2], Israel Arnedo[1], Miguel A. G. Laso[1], and Txema Lopetegi[1]

Abstract—This paper presents a design methodology that significantly increases the peak power handling capability (PPHC) of microstrip filters. The PPHC is limited in microstrip technology by the corona effect: a physical phenomenon caused by the ionization of the air in the presence of strong electric fields around the planar circuit. Microstrip filter with low electric field strength in the air increases the corona threshold level, resulting in high PPHC. Conventional stepped impedance (SI) filters, which consist of cascaded step-shaped elements, exhibit sharp discontinuities. These geometric edges amplify the electric field strength in the air, consequently reducing the corona threshold. Our research group has recently reported a new synthesis technique that introduces a smooth-profile (SP) conductor strip. This SP strip eliminates any sharp discontinuities and significantly reduces the strength of the electric field. This paper focuses on the examination of the high power performance of 7th-order SP and SI low-pass filters. The cut-off frequency (f_c) for both types of filters is set at 447.45 MHz, while the frequency for maximum stop-band rejection (f_o) is 1 GHz. The findings indicate that the SP filter shows a notable enhancement in peak power handling capability (PPHC), with gains of 2.48 dB and 4.80 dB observed at critical pressure and ambient pressure, respectively.

1. INTRODUCTION

Microstrip circuits have been widely used in a large number of applications, ranging from biomedical to satellite telecommunications. Their low volume, weight, and cost make them an attractive solution for designing multiple passive components such as dividers, couplers, and filters. In contrast to stripline technology, microstrip technology offers a simpler approach for building multifunctional devices [1]. Recent advances in material science have given rise to high-k substrates, which are helping researchers to design low-loss microstrip circuits. Moreover, solid-state power amplifier (SSPA) has made it possible to use microstrip technology at the outer stages of high-power transmitters. Therefore, particular consideration must be given to the power handling capabilities of the microstrip circuits.

Multipactor and ionization breakdowns are two major factors affecting the high-power operation of microwave devices. In RF and microwave components, cosmic rays create free electrons that accelerate under the electric field [2], strike the surfaces of the device, and generate secondary electrons in vacuum. Conditions may arise whereby these secondary electrons get exponentially multiplied; this effect is commonly known as multipactor breakdown or multipaction [3, 4]. On the other hand, the ionization breakdown or the Corona effect [5–8] is a process of converting an isolated gas into a conducting plasma. The presence of a strong electric field can lead to a substantial increase in electron density, resulting in a gas discharge. This discharge has the potential to damage individual components or even the entire

Received 6 April 2023, Accepted 17 May 2023, Scheduled 10 June 2023
* Corresponding author: Jamil Ahmad (jamil.ahmad@unavarra.es).
[1] Department of Electrical, Electronic and Communications Engineering, Institute of Smart Cities (ISC), Public University of Navarre (UPNA), Campus Arrosadia, Pamplona 31006, Spain. [2] European Space Research and Technology Centre, European Space Agency (ESTEC-ESA), AZ Noordwijk 2201, The Netherlands.

module. Multipaction and the corona effect are closely related phenomena in a sense that multipaction itself cannot damage the device unless there is a multipaction-gas ionization mechanism. Corona effect is more common in open devices like microstrip components, whereas multipactor is more prominent in closed structure like waveguides. Both these breakdowns need to be validated for ground-based components (e.g., base station transceivers) as well as space-bound components (e.g., satellite output filters, multiplexers). This paper is primarily focused on the corona breakdown for microstrip filters and technique to increase its threshold.

Microstrip filters are key components in any communication system at both the transmitter and receiver ends. A filter is a two-port network that passes the frequencies in the band of interest and rejects the unwanted frequencies. Among the classical filter design techniques [9–11], the insertion loss method has been widely used as a conventional synthesis approach based on discrete components. Since the discrete components are suitable only for low frequencies, distributed filter networks were developed to operate at high frequencies [12]. The equivalence between discrete elements and distributed networks is exact only at a single operating frequency. In a microstrip (distributed) filter, metal strips of different widths are cascaded to achieve the desired response. However, there are various demerits to the classical stepped-impedance technique, such as spurious bands, excitation of higher order modes, lack of control over out-of-band response, and poor selectivity. Our group reported on the concept of a smooth-profiled structure designed by employing inverse scattering synthesis techniques [13]. Although the sharp edges of the stepped-impedance filter were replaced by smooth transitions of the strip, the reported techniques were limited to only rational functions in terms of the reflection response with a long length of the device or to moderate maximum reflectivity (moderate maximum attenuations in the rejected band). To overcome these limitations and have full control over the length of the device, the "continuous layer peeling (CLP)" inverse scattering technique was proposed and used in [14]. It is based on peeling off successive layers of differential thickness, resulting in a smooth impedance profile with no sharp transitions.

2. CORONA ANALYSIS

The corona effect causes physical damage to the device by melting solder junctions and leaving distinct burn scars. This effect is characterized by its more energetic and localized nature than the multipactor phenomenon. Microstrip filters, being open structures surrounded by environmental gases, are more vulnerable to gas ionization breakdown. Due to the presence of fringing fields in open structures, it becomes crucial to evaluate the maximum strength of the electric field in the surrounding air. To calculate this, the voltage is determined through the line integral of the electric field in the cross-section of the strip conductor and the ground plane. The voltage varies along the length of the device and attains its peak value at the open circuit termination of microstrip resonator. For the microstrip line of characteristic impedance Z_0 and the input power P_0, the excitation voltage V_0 can be calculated as $V_0 = \sqrt{2Z_0P_0}$. In stepped-impedance resonators, the section with high impedance features a higher voltage value than the excitation voltage, as illustrated in Fig. 1. This concept is termed as voltage magnification, and the ratio V_{peak}/V_0 is called voltage magnification factor (VMF), which plays a vital

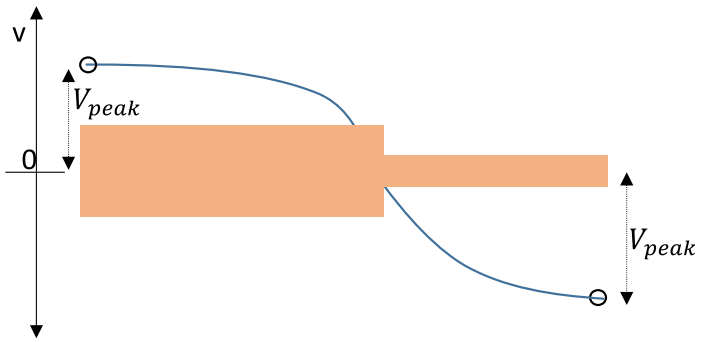

Figure 1. Voltage standing-wave for a stepped-impedance resonator.

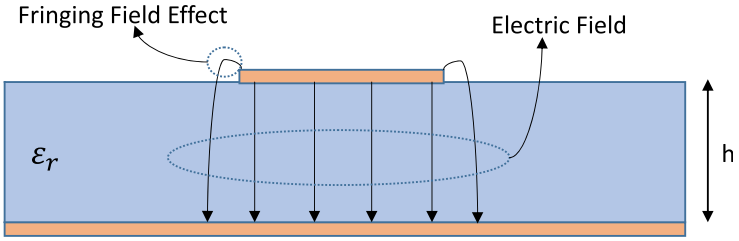

Figure 2. Electric field lines in the cross-section of a microstrip line, which demonstrates the fringing field effect.

role in analyzing PPHC. Generally, in a low-pass filter, the VMF is maximum at the cut-off frequency, while in a band-pass filter, it attains maximum at the central frequency of the passband.

Electric field lines, which originate just below the microstrip line, terminate at the ground conductor, as illustrated in Fig. 2. The electric field strength inside the dielectric is computed as $|E_{\text{peak}}| = \frac{V_{\text{peak}}}{h}$, where h is the thickness of the substrate. Since the microstrip is an open device, not all of the electric field is contained inside the substrate. Some portion of the electric field radiates in the air (fringing field effect), and this phenomenon gets more prominent at the sharp corners of the microstrip. At the dielectric-air interface, following boundary conditions must be satisfied:

$$\begin{aligned} \vec{n} \cdot \vec{D}_{\text{air}} = \vec{n} \cdot \vec{D}_{\text{dielectric}} &\Longrightarrow \vec{E}_{\text{air},n} = \varepsilon_r \cdot \vec{E}_{\text{dielectric},n} \\ \nabla \times \vec{E}_{\text{air}} = \nabla \times \vec{E}_{\text{dielectric}} &\Longrightarrow \vec{E}_{\text{air,tan}} = \vec{E}_{\text{dielectric,tan}} \end{aligned} \tag{1}$$

where n and tan refer to the normal and tangential components of the electric field ($\vec{E}$), respectively, and $\vec{D}$ denotes the electric flux density. According to the boundary conditions, the normal components of electric field in the air are ε_r times greater than the electric field confined inside the dielectric.

If the electric field in the air is strong enough, the neutral molecules of the air get ionized by releasing free electrons. The presence of these free electrons leads to an exponential growth of the electron density transforming air into a conducting plasma. This continuous growth of electron density ultimately leads to a gas discharge. The electric field strength ($|E_{\text{break}}|$) at which this ionization breakdown occurs can be semi-analytically approximated [5–8] for a pressure, p at a particular frequency, f by the following equation:

$$|E_{\text{break}}| = 3.75p\left(1 + \frac{4\pi^2 f^2}{25 \times 10^{18}}\right)^{1/2} \times \left(\frac{10^6}{p^2 L_{eff}^2} + 6.4 \times 10^4 + \frac{20}{p\tau_p}\right)^{3/16} \tag{2}$$

where L_{eff} is the effective diffusion length between the free electrons; τ_p is the pulse length; and the pressure, p, is defined as $p = p_0\left(\frac{273}{273+T_0}\right)$, where p_0 is the air pressure in Torr, and T_0 is the temperature in degree Celsius.

During spacecraft launching, the pressure varies from ambient to vacuum. Consequently, it becomes crucial to characterize space-borne components to withstand this pressure range. The power analysis performed along the pressure axis is commonly known as the "Paschen curve", as depicted in Fig. 3. At ambient pressure, the average random collision distance of gas particles, (the mean free path) is very small, and the free electrons cannot make a powerful collision with gas molecules to knockout further electrons. As a result, a high PPHC is achieved at ambient pressure. As the pressure decreases, the free electrons get enough space to make a powerful impact to ionize the gas particles; this in turn reduces the PPHC. This trend persists until a specific pressure, known as the "critical pressure," is reached, which corresponds to the minimum PPHC. When the pressure further drops below the critical pressure, the mean free path becomes significantly large. Consequently, the probability of gas ionization decreases, resulting in an exponential increase in the PPHC.

For pressures higher than 100 mbar, the threshold of air ionization can be estimated by the following equation [15]:

$$|E_{\text{break}}| = 42.7 \times \sqrt{p^2 + 2f^2} \tag{3}$$

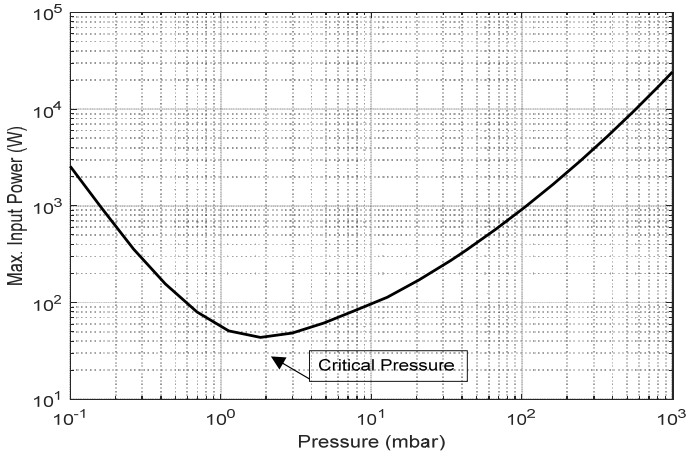

Figure 3. Paschen curve for air ionization breakdown (Corona effect).

where f is the frequency in gigahertz, and p is pressure in Torr. A general rule accepted within the microwave engineering community is to combine the aforementioned formula (3) with the maximum electric field strength calculated by a full-wave simulator. This approach aims to estimate a conservative value of PPHC in order to ensure the safe operation of the device.

3. CLASSICAL FILTER THEORY

A microstrip stepped-impedance periodic filter can be designed by using classical filter design theory [16, 17]. The classical filter is constructed by cascading N line-sections, each having the same electrical length but different characteristic impedances, with an additional input and output line-section corresponding to the port impedances. The transmission matrix of a unit element having characteristic impedance Z_0 is calculated by Equation (4) using the $[ABCD]$ transfer matrix [18–20]. The distributed network is derived by invoking Richards' transformation [21] as illustrated in Fig. 4.

$$\begin{bmatrix} A & B \\ C & D \end{bmatrix}_{UE} = \frac{1}{\sqrt{1-t^2}} \begin{bmatrix} 1 & Z_0 t \\ t/Z_0 & 1 \end{bmatrix} \tag{4}$$

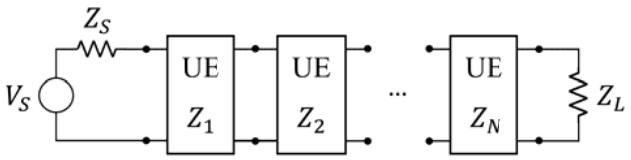

Figure 4. Commensurate-line distributed prototype represented in the Richards' transformation domain as a cascade of N UEs (unit elements).

By multiplying the transfer matrices of the N UEs, the overall transmission coefficient of a lossless two-port network can be derived by using following expression:

$$S_{21}(t) = \frac{\left(1-t^2\right)^{N/2}}{P_N(t)} \tag{5}$$

where $P_N(t)$ is a strictly Hurwitz polynomial in t of order N.

To determine the order of the Chebyshev filter (N) based on filter's specifications, such as minimum insertion loss ($|S_{21}|_{\min}$), frequency of maximum rejection (f_0), return loss, and cut-off frequency (f_c),

following formula (6) is used:

$$N = \frac{\operatorname{acosh}\sqrt{\left(\frac{1}{|S_{21}|^2_{\min}} - 1\right) \cdot \left(10^{\frac{RL}{10}} - 1\right)}}{\operatorname{asech}\left(\frac{1}{\alpha}\right)} \tag{6}$$

where $\alpha = 1/\sin\theta_c$, θ_c being the electrical length of the commensurate lines at the cut-off frequency, f_c.

The characteristic impedances of N unit-elements are calculated, which lead to stepped-impedance profile of the conventional filter. Commercially available software ADS Linecalc$^{\text{TM}}$ is employed to extract the microstrip widths for the corresponding impedance profile. Linecalc$^{\text{TM}}$ requires f_c and substrate's specifications, i.e., height (h), relative permittivity, (ϵ_r) and loss tangent ($\tan\delta$) to perform this task accurately. It results in a classical stepped-impedance filter, featuring equal electrical length in all the unit element sections and known as commensurate line filter. The classical stepped-impedance filter with cascaded unit elements features sharp edges with 90-degree transitions. These sharp edges concentrate the electric field at these regions, thereby intensifying the electric field's strength. The high electric field at the corners ionizes the gas molecules (i.e., air), and corona discharge appears at low power levels that subsequently reduces the PPHC of the filter.

4. SMOOTH-PROFILED FILTER

The threshold of the corona breakdown can be improved by rounding the sharp corners of the device. The presence of smooth transitions in the strip width reduces the electric field strength, thereby enhancing the PPHC [22]. The classical stepped-impedance filter serves as foundation for designing the novel smooth-profile microstrip filter, which maintains the same physical length as the conventional filter. The S-parameter response of the stepped-impedance filter is periodic, with repeated rejection bands at regular intervals. This response is modified by nullifying the spurious stopbands of the frequency response, as depicted in Fig. 5. This modification ensures a spurious-free target frequency response, which serves as input to the layer-peeling algorithm.

The inverse scattering layer peeling procedure was initially developed in the time domain by Feced et al. [23] for the synthesis of fiber Bragg gratings in the optical frequency range. Subsequently,

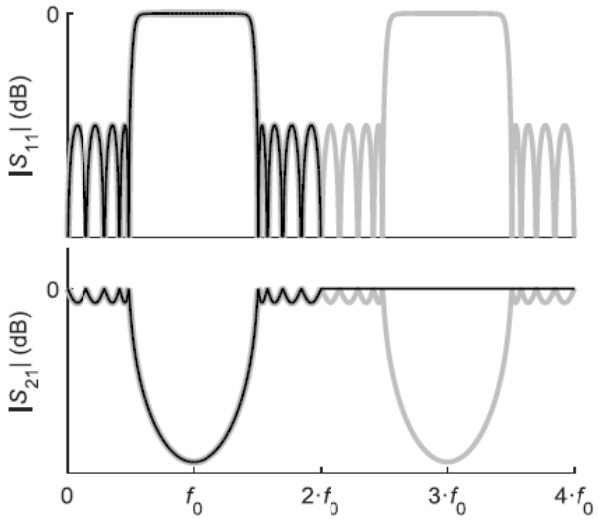

Figure 5. Scheme of the frequency response of a generic Nth-section classical Chebyshev periodic filter (gray line) and its transformation to the target frequency response used in the continuous layer peeling (CLP) synthesis method (black line).

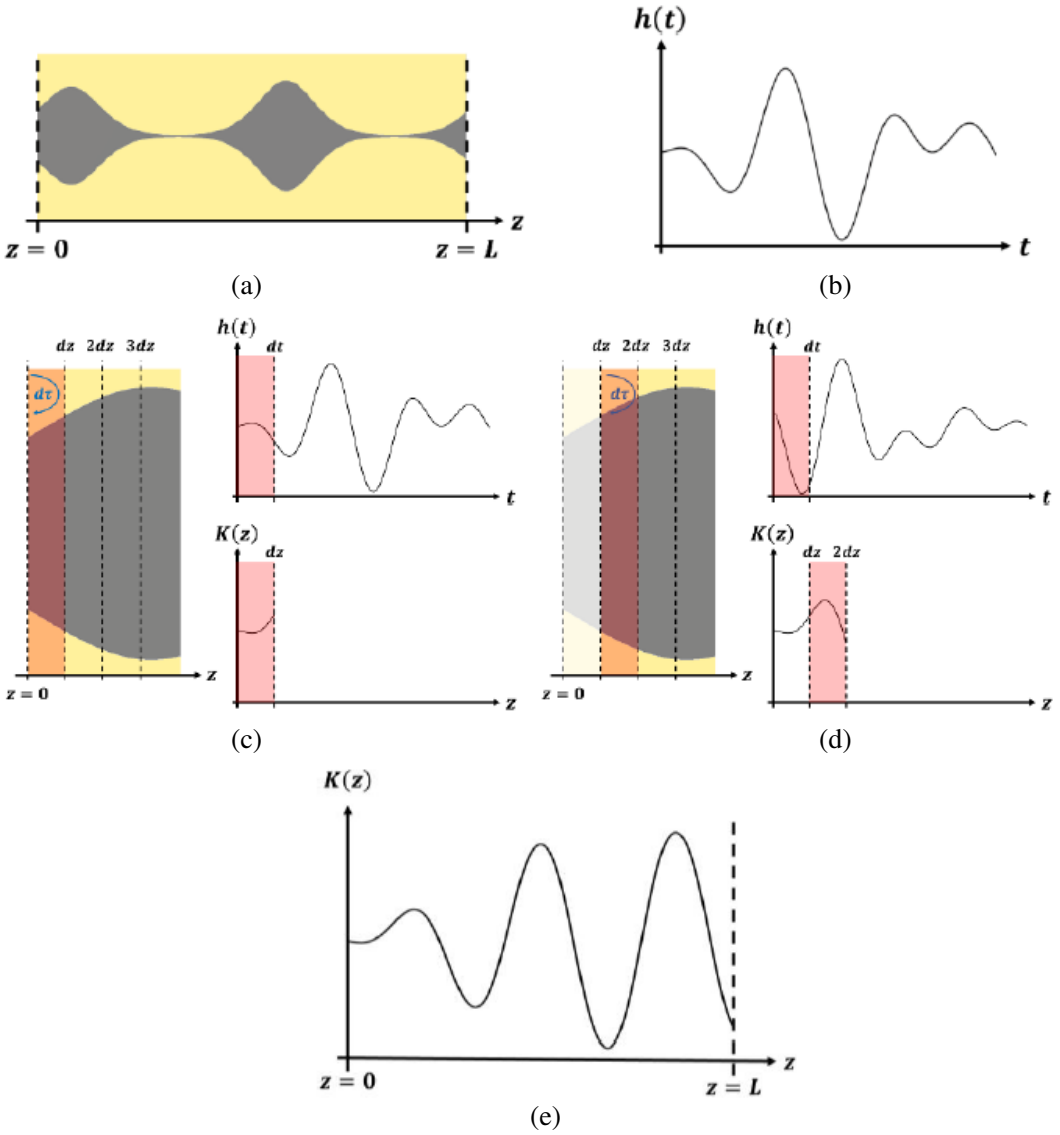

Figure 6. Schematic representation of the CLP method: (a) unknown physical structure intended to be synthesized by calculating its coupling coefficient with CLP, (b) target impulse response in reflection, $h(t)$, (c) the first dt instant of $h(t)$ must be governed only by the first dz layer of the device due to the causality principle and thus, it is possible to calculate the coupling coefficient, $K(z)$, for dz, (d) once the first layer is peeled-off, a new $h(t)$ must be accomplished by the rest of the device, and by applying the same procedure, the coupling coefficient between dz and $2dz$ can be calculated, (e) once all layers have been peeled-off, the coupling coefficient of the whole structure is determined.

Skaar [24, 25] and Poladian [26, 27] translated this technique into the frequency domain. Building upon these advancements, our group applied the concept of inverse scattering layer peeling to the RF and microwave frequencies. This adaptation allowed for the synthesis and design of RF and microwave components using this powerful technique. The continuous layer peeling (CLP) algorithm divides the length of the device into infinitesimally thin layers. At the input port ($z = 0$), when an ideal impulse excites the device, the reflection response of the first layer in the time domain (forward and backward time interval) is determined. This process is repeated iteratively for each layer. Fig. 6 illustrate the schematic representation of this algorithm. Smooth-profile filter extracted by the CLP algorithm offer two advantages: (1) the sharp corners of the SI filter are transformed into smooth transitions, which

prevent the field accumulation, and increase the PPHC [22]; (2) since the CLP algorithm provides an exact solution, a spurious-free frequency response is achieved.

A brief summary of the design methodology is as follows:

Step 1: For the given filter specifications, the order of the filter, N is calculated by (6).

Step 2: The impedance values of the N unit element sections are calculated using the $[ABCD]$ transfer matrix using (4).

Step 3: The frequency response of the SI device is computed by multiplying the transfer matrices of the N cascaded unit elements by employing Equation (5).

Step 4: The frequency response obtained in Step 3 features periodic rejection bands. The S_{11} response of the SI is truncated by nullifying the S_{11} parameters beyond $2f_0$. It results in an ideal frequency response with no spurious rejection bands, serving as the target response for the CLP synthesis algorithm.

Step 5: In the modified target frequency response, the CLP algorithm is applied to synthesize the coupling coefficient. Initially, the CLP method is applied at the origin of the device ($z = 0$), considering the first infinitesimal layer, to get the coupling coefficient $K(0)$ by using (7).

$$K(z=0) = -\frac{4}{\pi}\int_0^\infty \mathrm{Re}\left\{S_{11}(\beta)\right\} \cdot d\beta \tag{7}$$

Step 6: Once the initial coupling coefficient is evaluated, the Riccati equation (8) is used to propagate the reflection coefficient along the first layer of the device. Now, the first layer is peeled off and the origin of the device is shifted to the next layer. The succeeding value of the coupling coefficient can be calculated using (7). Following iteratively, i.e., propagating the target spectrum with (8) and calculating the next value of the coupling coefficient by utilizing (7), the entire coupling coefficient $K(z)$ of the smooth profile device is synthesized.

$$\frac{d\rho}{dz} = 2 \cdot j \cdot \beta \cdot \rho + K \cdot \left(1 - \rho^2\right) \tag{8}$$

Step 7: Finally, the characteristic impedance profile corresponding to the coupling coefficient calculated in Step 6 is computed by using the analytical expression (9).

$$Z_0(z) = Z_0(0) \cdot e^{-2\int_0^z K(g)\cdot dg} \tag{9}$$

where $Z_0(0)$ is the value of the characteristic impedance at the input port, and g is a dummy variable to calculate the integral. A macro file is created to extract the width profile of the strip in ADS Linecalc. Fig. 7 illustrates the impedance profiles of both the stepped-impedance and the smooth-profiled seventh order Chebyshev filter.

5. DESIGN EXAMPLE

In order to compare the power handling performance of the stepped-impedance (SI) and smooth-profile (SP) techniques, two prototypes (SI, SP) are designed with the design specifications listed in Table 1.

The impedance and strip-width profiles of both filters are depicted in Fig. 7 and Fig. 8, respectively. The smooth profile design prototype is fabricated, and its photograph is shown in Fig. 9. Both prototypes are simulated in CST$^{\mathrm{TM}}$ and the corresponding S-parameter response is presented in Fig. 10. The SP filter is numerically analyzed using couple mode theory [13]. The measurement of the fabricated smooth-profiled prototype is performed with an Agilent$^{\mathrm{TM}}$ 8722 Vector Network Analyzer and the results are presented in Fig. 11. The excellent agreement found among the target, simulation, analyzed, and measurement responses confirms the accuracy of the continuous layer-peeling (CLP) algorithm. The target specifications are achieved in measurement with remarkable accuracy: the central frequency of the stopband, $f_0 = 1\,\mathrm{GHz}$, cut-off frequency, $f_c = 447.45\,\mathrm{MHz}$, maximum rejection is 30 dB, and the return loss level is better than 20 dB. The small discrepancies found can be attributed to the fabrication tolerances, uncertainty in the dielectric constant of the substrate, and the connectors.

Since the voltage magnification is maximum at the cut-off frequency [28], the electric fields of both prototypes are computed at the cut-off frequency (0.447 GHz). In the stepped-impedance filter, it is

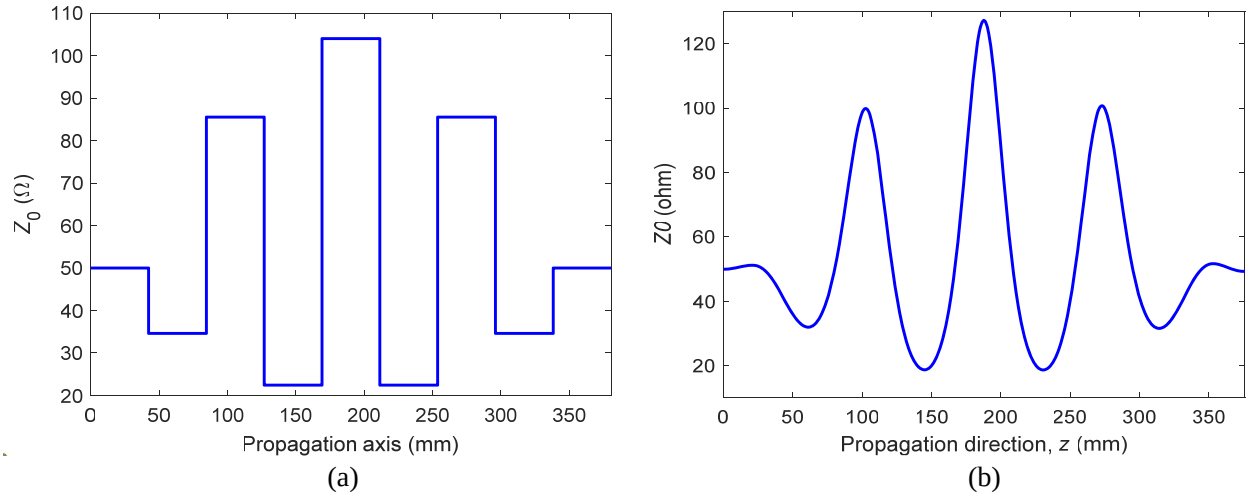

Figure 7. Characteristic impedance along the propagation direction: (a) Stepped-impedance filter, (b) smooth-profiled filter.

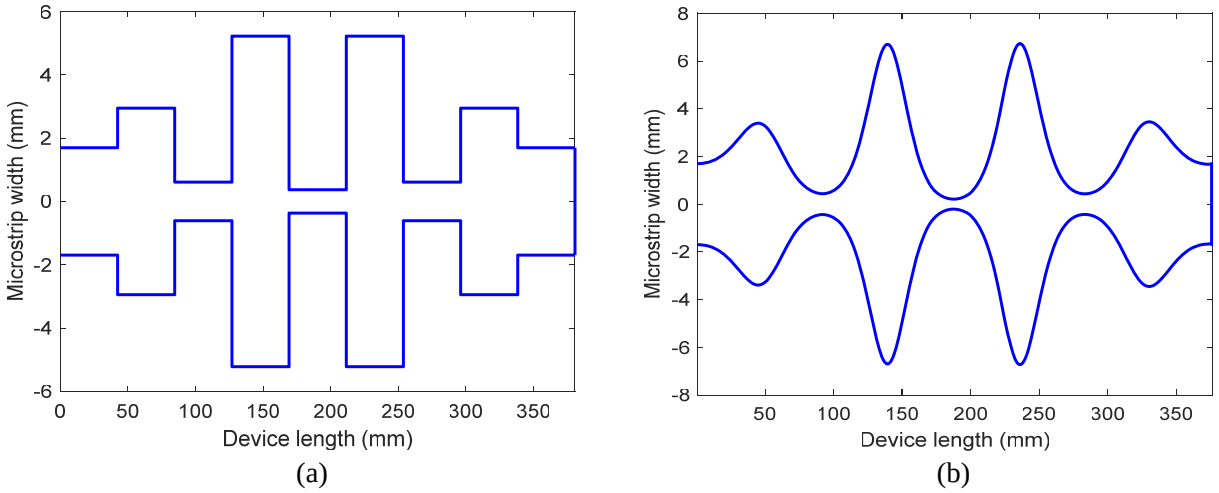

Figure 8. Microstrip width profile along the propagation direction: (a) Stepped-impedance filter, (b) smooth-profiled filter.

Table 1. Specifications of designed prototypes.

Frequency Specifications	Cutoff frequency, f_c	0.447 GHz
	Frequency of maximum rejection, f_0	1 GHz
Insertion Loss		30 dB
Return Loss, RL		20 dB
Filter Order, N		7
Substrate		Roger 3035, $\varepsilon_r = 3.5$
Substrate thickness, h		1.524 mm

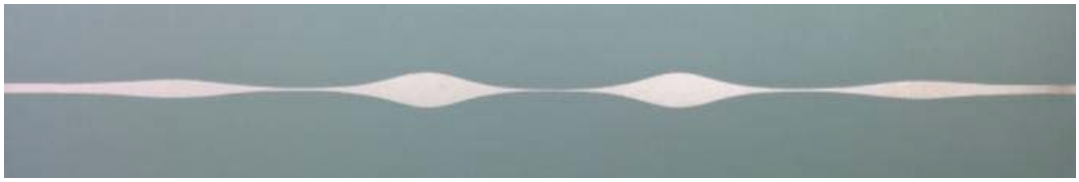

Figure 9. Photograph of fabricated smooth-profile filter as design example.

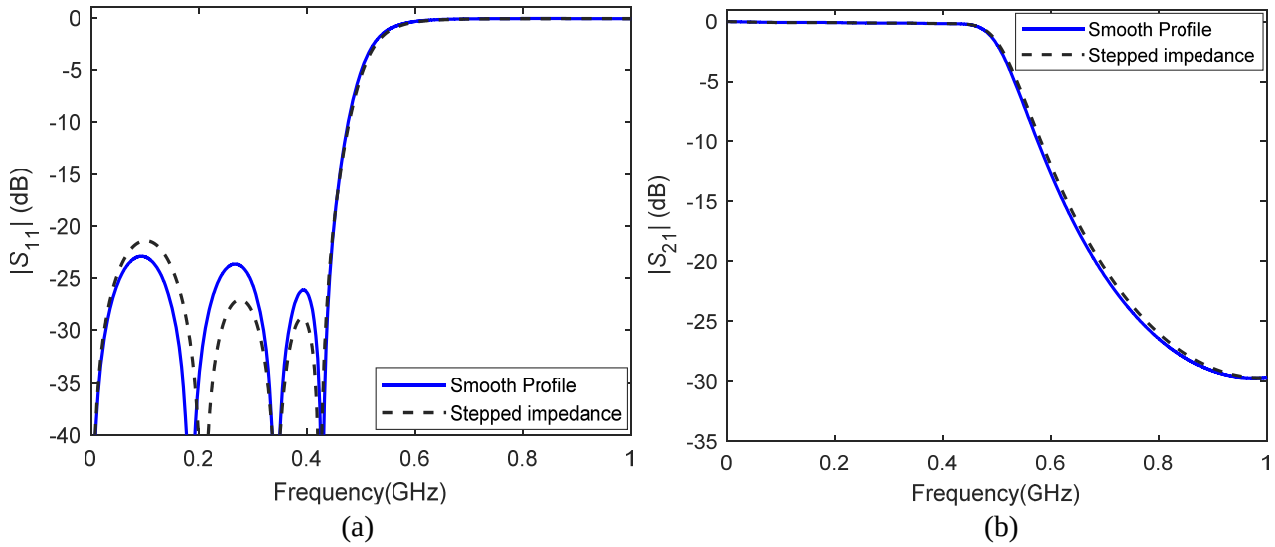

Figure 10. CST^{TM} simulated frequency response of the smooth-profile filter (solid line) and stepped-impedance filter (dash line)): (a) S_{11} response, (b) S_{21} response.

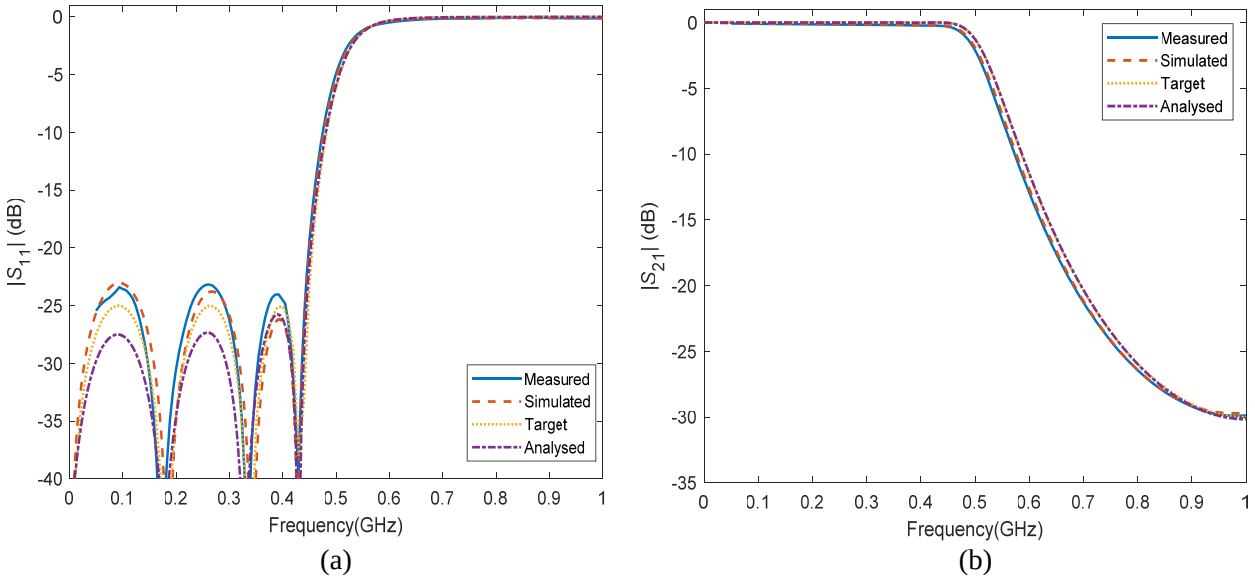

Figure 11. S-parameter results of the smooth-profile filter-measured response (solid line), simulated response (dashed line), target response (dotted line), and analyzed response (dashed-dot line): (a) S_{11} response, (b) S_{21} response.

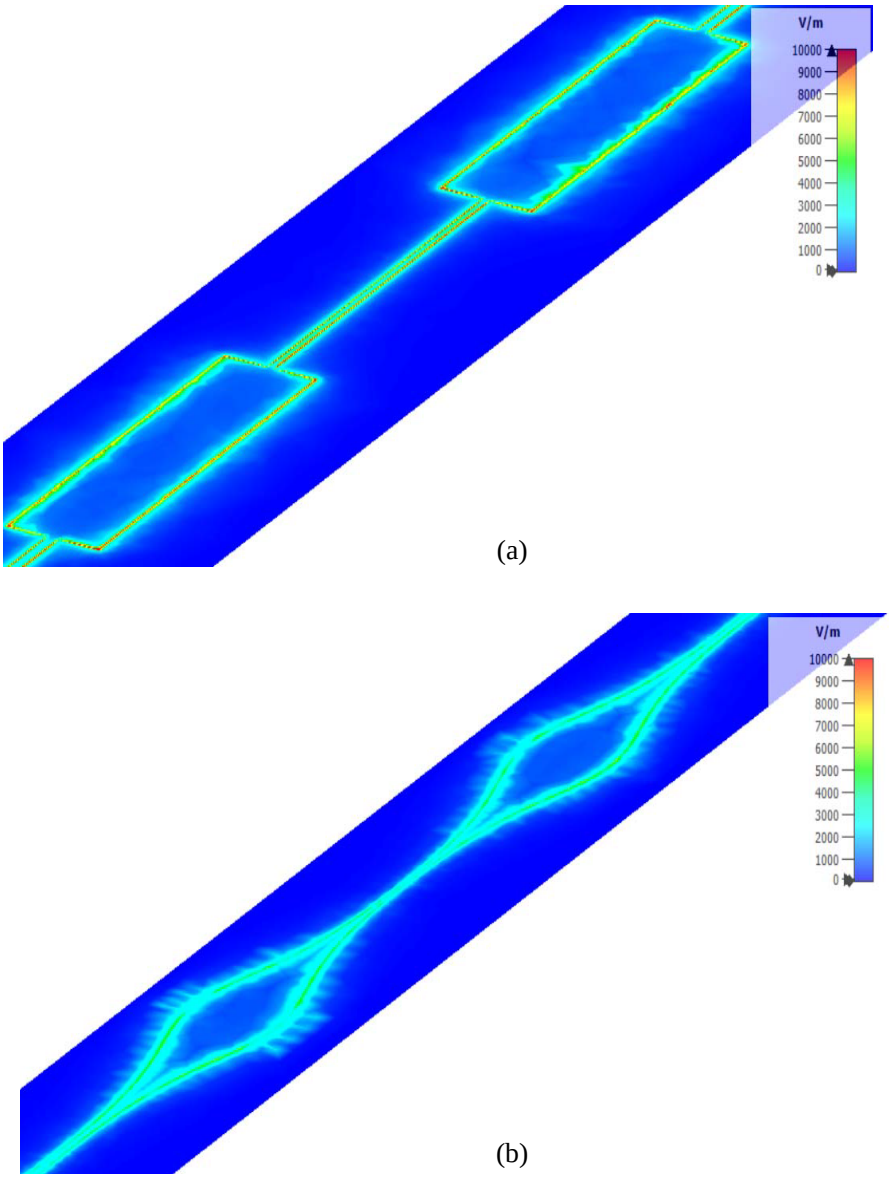

Figure 12. 3D-electric field pattern along the device for (a) the stepped-impedance filter, and (b) the smooth-profile filter.

observed that most of the electric field is accumulated at the sharp corners of the strip, whereas in the smooth-profiled filter, the presence of smooth transitions avoids the concentration of the electric fields. To visualize this effect, the electric field patterns for both the SI and SP filters are presented in Fig. 12.

6. PEAK POWER HANDLING CAPABILITY (PPHC)

The electric field calculated at the cut-off frequency of the filter in CST^{TM} is exported to the commercial software tool SPARK3D^{TM}. For air pressure sweep, 0.1 mbar–1000 mbar at ambient temperature (293 K), the corona breakdown of the device is analyzed. Inspecting the corona breakdown results presented in Fig. 13, the graphs reveal that the PPHC is much better for the smooth-profile filter compared to its stepped-impedance counterpart. The smooth-profile filter's corona breakdown threshold at critical pressure (1.13 mbar) is 35.81 W, which is 2.47 dB higher when compared with 20.25 W for the stepped-impedance filter at the same pressure. Similarly, at ambient pressure (1000 mbar), the smooth-

Table 2. Corona breakdown values at critical and ambient pressure.

	Stepped impedance filter	Smooth profile filter
PPHC at critical pressure (1.13 mbar)	20.25 W	35.81 W
PPHC enhancement at critical pressure	2.47 dB	
PPHC at ambient pressure (1000 mbar)	30.5 KW	92.2 KW
PPHC enhancement at ambient pressure	4.80 dB	

Table 3. Comparison of the corona breakdown improvement techniques in microstrip technology.

Technique	Filter's design Topology	Filter's order (N)	ε_r	f_o (Frequency of maximum rejection in GHz)	Improvement in Corona Threshold at ambient pressure
Commercial anti-corona lacquer	coupled-resonator BPF*	3	3.6	1.6	1.1 dB
Rounded-cornered resonator	coupled-resonator BPF	3	3.6	1.6	2.12 dB
Cover-ended resonator	coupled-resonator BPF	3	3.6	1.6	3.1 dB
Smooth-profiled microstrip (This work)	continuous layer peeling method (CLP) LPF^	7	3.5	1	4.8 dB

* Band pass filter ^ Low pass filter

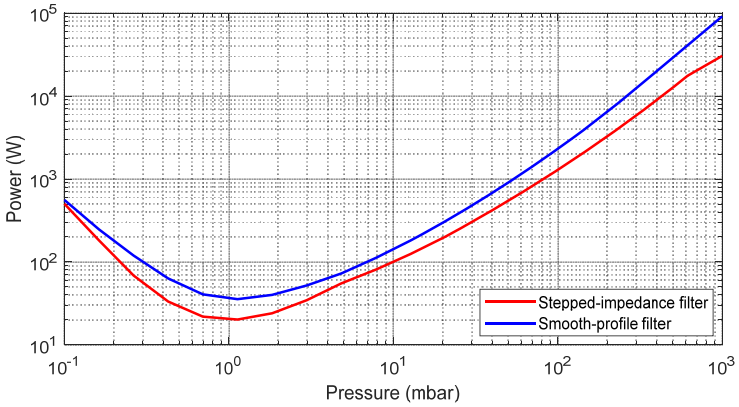

Figure 13. Corona discharge breakdown (Paschen curve) simulated in Spark 3D at $f_c = 447.45$ MHz.

profile filter can handle power up to 92.2 kW, whereas the stepped impedance filter can manage only 30 kW, with a significant enhancement of 4.80 dB. A comparison of the PPHC values for the smooth-profiled and stepped-impedance filters, both at critical and ambient pressures, is given in Table 2.

It can be observed from Fig. 13 that if the pressure reduces from ambient pressure (1000 mbar) towards the critical pressure (1.13 mbar), the PPHC (air ionization threshold) of both devices decline along the pressure axis until the minimum PPHC is achieved at critical pressure. When the pressure is

further decreased below the critical pressure, the devices experience a significant increase in PPHC. However, throughout the whole pressure range (0.1 mbar–1000 mbar) the Paschen curve of SP is consistently leading the SI device with the highest improvement (4.80 dB) at ambient pressure, denoting a higher power handling capability of the smooth-profile filter.

In literature, there are very few papers related to PPHC in microstrip technology. To the author's knowledge, three approaches have been reported to improve the corona breakdown threshold: (1) rounded-cornered microstrip resonators [22]; (2) cover-ended microstrip resonators [29]; (3) commercial anti-corona lacquer [29]. A brief comparison of PPHC improvement techniques is presented in Table 3.

7. CONCLUSION

In this paper, the PPHCs of two filter design techniques, the classical stepped-impedance (SI) filter and a smooth-profile (SP) filter are presented. The SP filter is obtained by applying an inverse scattering synthesis method that avoids the abrupt impedance transitions. This approach has two advantages; it suppresses periodic stop bands and lowers the electric field intensity along the device that results in improved peak power handling capability (PPHC) of the filter. The phenomenon of electric field strength of both SI and SP is also presented; SI exhibits high electric field concentration at sharp corners. Corona analysis is performed in SPARK 3D$^{\text{TM}}$, which clearly shows that the SP filter can handle more peak power than the SI filter with an improvement of 2.47 dB and 4.8 dB at critical and ambient pressures respectively. Furthermore, the SP approach is compared with three other PPHC improvement techniques, and SP is found to be exceptional among these methods.

ACKNOWLEDGMENT

This work was supported by the Spanish Ministerio de Ciencia e Innovación — Agencia Estatal de Investigación (MCIN/AEI/10.13039/501100011033) under Project PID2020-112545RB-C53. Jamil Ahmad also acknowledges the funding received through the PRE2018-085491 grant.

REFERENCES

1. Cameron, R. J., C. M. Kudsia, and R. R. Mansour, *Microwave Filters for Communication Systems*, 2nd Edition, Wiley, Somerset, U.K., 2018.
2. Maxwell, J. C., *A Treatise on Electricity and Magnetism*, 3rd Edition, Vol. 2, 68–73, Clarendon, Oxford, 1892.
3. Woode, A. and J. Petit, "Diagnostic investigations into the multipactor effect, susceptibility zone measurements and parameters affecting a discharge," *ESTEC* Working Paper 1556, Eur. Spacy Agency, Noordwijk, The Netherlands, Nov. 1989.
4. Anderson, D., U. Jordon, M. Lisak, T. Olsson, and M. Ahlander, "Microwave breakdown in resonators and filters," *IEEE Trans. Microw. Theory Techn.*, Vol. 47, No. 12, 2547–2556, Dec. 1999.
5. MacDonald, A. D., *Microwave Breakdown in Gases*, Wiley, New York, NY, USA, 1966.
6. Raizer, Y. P., *Gas Discharge Physics*, Springer, Berlin, Germany, 1991.
7. Woo, R., "Final report on RF voltage breakdown in coaxial transmission lines," *Tech. Rep. 32-1500*, Jet Propulsion Lab, CA, U.S.A., Oct. 1970.
8. Puech, J., M. Merecki, D. Anderson, M. Buyanova, D. Doroshkina, U. Jordan, L. Lapierre, M. Lisak, V. E. Semenov, J. Sombrin, and R. Udilijak, "Microwave discharge research activities within the contest of the Chalmers University (Sweden)/Institute of Applied Physics (Russia)/CNES (France) project," *Proc. 4th Int. Workshop on Multipactor, Corona and Passive Intermodulation in Space RF Hardware (MULCOPIM)*, Sep. 2003.
9. Levy, R. and S. B. Cohn, "A history of microwave filter research, design, and development," *IEEE Trans. Microw. Theory Tech.*, Vol. 32, No. 9, 1055–1067, Sept. 1984.
10. Levy, R., R. V. Snyder, and G. Matthaei, "Design of microwave filters," *IEEE Trans. Microw. Theory Tech.*, Vol. 50, No. 3, 783–793, Mar. 2002.

11. Hunter, I. C., L. Billonet, B. Jarry, and P. Guillon, "Microwave filters — Applications and technology," *IEEE Trans. Microw. Theory Tech.*, Vol. 50, No. 3, 794–805, Mar. 2002.
12. Matthaei, G., L. Young, and E. M. T. Jones, *Microwave Filters, Impedance-matching Networks, and Coupling Structures*, Artech House, Inc., 1980.
13. Arnedo, I., I. Arregui, M. Chudzik, F. Teberio, A. Lujambio, D. Benito, T. Lopetegi, and M. A. G. Laso, "Direct and exact synthesis: Controlling the microwaves by means of synthesized passive components with smooth profiles," *IEEE Microwave Magazine*, Vol. 16, No. 4, 114–128, May 2015.
14. Arnedo, I., M. Chudzik, J. M. Percaz, I. Arregui, F. Teberio, D. Benito, T. Lopetegi, and M. A. G. Laso, "Synthesis of one dimensional electromagnetic bandgap structures with fully controlled parameters," *IEEE Trans. Microw. Theory Techn.*, Vol. 65, No. 9, 3123–3134, Sept. 2017.
15. Woo, W. and J. DeGroot, "Microwave absorption and plasma heating due to microwave breakdown in the atmosphere," *IEEE Phys. Fluids*, Vol. 27, No. 2, 475–487, 1984.
16. Baher, H., *Synthesis of Electrical Networks*, John Wiley & Sons, New York, NY, USA, 1984.
17. Ozaki, H. and J. Ishii, "Synthesis of a class of strip-line filters," *IRE Trans. Circuit Theory*, Vol. 5, No. 2, 104–109, Jun. 1958.
18. Wenzel, R. J., "Exact design of TEM microwave networks using quarter-wave lines," *IEEE Trans. Microw. Theory Tech.*, Vol. 12, No. 1, 94–111, Jan. 1964.
19. Minnis, B. J., *Designing Microwave Circuits by Exact Synthesis*, Artech House, Norwood, MA, USA, 1996.
20. Carlin, H. J. and P. P. Civalleri, *Wideband Circuit Design*, CRC Press, Boca Raton, FL, USA, 1998
21. Richards, P. I., "Resistor-transmission-line circuits," *Proc. IRE*, Vol. 36, No. 2, 217–220, Feb. 1948.
22. Morales-Hernández, A. M., M. Á. Sánchez-Soriano, S. Marini, et al., "Increasing peak power handling in microstrip bandpass filter by using rounded-end resonantors," *IEEE Microw. Wireless Compon. Lett.*, Vol. 31, No. 3, 237–240, Mar. 2021.
23. Feced, R., M. N. Zerbas, and M. A. Muriel, "An efficient inverse scattering algorithm for the design of nonuniform fiber bragg gratings," *IEEE J. Quantum Electron.*, Vol. 35, No. 8, 1105–1115, Aug. 1999.
24. Skaar, J., "Synthesis and characterization of fiber Bragg gratings," PhD Dissertation, The Norwegian University of Science and Technology, Norway, 2000.
25. Skaar, J., L. Wang, and T. Erdogan, "On the synthesis of fiber bragg gratings by layer peeling," *IEEE J. Quantum Electron.*, Vol. 37, No. 2, 165–173, Feb. 2001.
26. Poladian, L., "Simple grating synthesis algorithm," *Opt. Lett.*, Vol. 25, No. 11, 787–789, Jun. 2000.
27. Poladian, L., "Simple grating synthesis algorithm: Errata," *Opt. Lett.*, Vol. 25, No. 18, 1400–1400, Sept. 2000.
28. Sánchez-Soriano, M. Á., Y. Queré, V. Le Saux, et al., "Peak and average power handling capability of microstrip filters," *IEEE Trans. Microw. Theory Techn.*, Vol. 67, No. 8, 3436–3448, Aug. 2019.
29. Morales-Hernández, A., M. Á. Sánchez-Soriano, S. Marini, et al., "Enhancement of corona discharge thresholds in microstrip bandpass filters by using cover-ended resonators," *International Journal of Microwave and Wireless Technologies*, Vol. 13, 708–718, Apr. 2021.